JOURNAL OF SPACECRAFT AND ROCKETS
Vol. 39, No. 1, January–February 2002

Dynamic Stability of Blunt Atmospheric Entry Configurations

Gerald L. Winchenbach* and Gary T. Chapman†
University of Florida, Shalimar, Florida 32579
Wayne H. Hathaway‡
Arrow Tech Associates, So., Burlington, Vermont 05403
Alvin Ramsey§
University of California, Berkeley, Berkeley, California 94720
and
Claude Berner¶
French-German Research Institute, F-68301 Saint-Louis, France

A series of free flight-test programs conducted on scale models of various blunt atmospheric entry configurations is discussed. Most of these tests were conducted in the Aeroballistic Research Facility, located at Eglin Air Force Base, Florida. The tests for Reynolds-number effects were conducted in the Hypervelocity Free-Flight Aerodynamic Facility located at NASA Ames Research Center at Moffett Field, California. Because these blunt atmospheric entry shapes have a tendency to experience small angle-of-attack dynamic instabilities leading to limit-cycle motions, the primary purpose of the tests was to determine the dynamic stability characteristics of the configurations. Although all of the aerodynamic parameters were obtained during these tests and are presented in the corresponding references, only the dynamic stability results are discussed. The tests were conducted from subsonic to supersonic Mach numbers, 0.7 to 3.5, Reynolds numbers from 0.27×10^6 to 6.97×10^6, and for angles of attack up to 40 deg.

Nomenclature

A	=	reference area, $\pi D^2/4$, mm^2
Cmq	=	damping-in-pitch derivative, 1/rad
C_N	=	normal force coefficient
$C_{N\alpha}$	=	normal force derivative, 1/rad
C_X	=	force coefficient, x direction
D	=	model diameter, reference length, mm
I_x, I_y	=	moments of inertia about the x and y axes, g cm^2
L	=	model length, mm
l, m, n	=	moments about the x, y, z axes
M	=	Mach number
V	=	model velocity, m/s
X	=	down range distance traveled, m
Xcg	=	distance from model nose to center of gravity, mm
$\bar{\alpha}$	=	total angle of attack, deg
ρ	=	air density, g/cm^3

Introduction

PLANETARY atmospheric entry configurations typically have blunt conical noses with various afterbody shapes dictated by mission requirements. The blunt conical noses are designed to utilize the aerodynamic drag in order to achieve a certain deceleration profile as the vehicle enters the planetary atmosphere. This deceleration is required in order to ensure a certain velocity either at impact or upon parachute deployment. Figure 1 shows a typical mission profile. Unfortunately, these blunt bodies tend to experience low-angle-of-attack dynamic instabilities[1,2] in the high supersonic to transonic Mach-number range. These dynamic instabilities can lead to angular motions that frequently develop into limit cycles,[3] and this is the focus of the present paper. If the magnitude of the limit cycle is relatively small, i.e., a few degrees, the limit cycle might not cause problems associated with completing the mission. However if this limit cycle is large, the vehicle could entangle itself in the parachute lines, thereby losing the vehicle, or the impact angle could be too large for the vehicle to successfully perform its mission upon landing. Therefore, the determination of the vehicle's dynamic stability characteristics is important during the mission planning stage.

Flight testing subscale models has proven to be a fast and inexpensive method of determining the low-angle-of-attack dynamic stability characteristics of these configurations. This paper discusses the dynamic stability test results obtained from six different configurations encompassing 83 flights in two different free-flight test facilities.

Aerodynamic Testing

Facilities and Data-Reduction Techniques

The majority of the tests discussed herein were conducted in the Aeroballistic Research Facility (ARF).[4] The U.S. Air Force Research Laboratory (AFRL) Munitions Directorate in partnership with the University of Florida Graduate Engineering and Research Center manages and operates this facility. The tests for the effects of Reynolds number were conducted in the NASA Ames Research Center's Hypervelocity Free-Flight Aerodynamic Facility (HFFAF).[5] In both facilities the aerodynamic and stability characteristics of a test item are determined from the measurement of the test item's spatial and angular orientations observed during the free flight.[6]

The ARF is an atmospheric facility and has a 207-m instrumented length. This facility has a 3.66-m square cross section for the first 69 m and a 4.88-m square cross section for the remaining length. Orthogonal photographs of the model's shadow are obtained at 50 instrumentation sites and then used to determine the spatial position and angular orientation of the test model at each location. The HFFAF is a variable pressure facility 25 m long with 16 orthogonal shadowgraph stations. In both facilities the film reading process and the determination of the discrete times, positions, and orientations are performed using the Comprehensive Automated Data

Received 15 June 2000; revision received 31 August 2001; accepted for publication 6 September 2001.

*Senior Researcher, Graduate Engineering and Research Center, 1305 N. Poguito Road. Associate Fellow AIAA.
†Adjunct Professor, Graduate Engineering and Research Center, 1305 N. Poguito Road. Fellow AIAA.
‡Vice President of Engineering. Senior Member AIAA.
§Ph.D. Candidate. Student Member AIAA.
¶Scientist. Member AIAA.

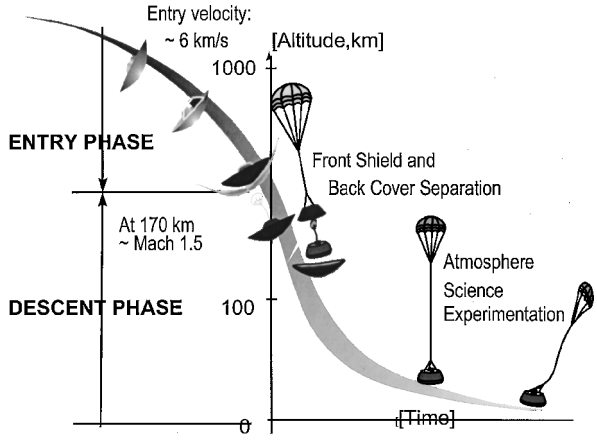

Fig. 1 Typical mission profile.

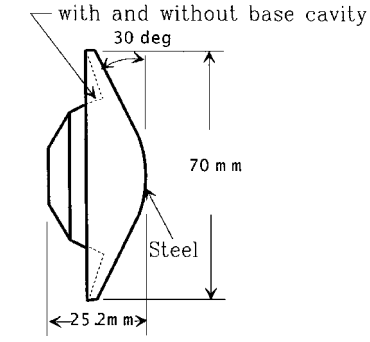

a) Huygens Probe

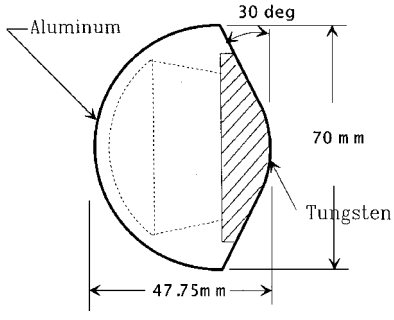

b) Huygens Probe with hemispherical base

Fig. 2 Sketch of Huygens Probe and probe with hemispherical base.

Reduction and Analysis System (CADRA).[7] The analysis process for the experimentally measured trajectories as obtained from the ARF is accomplished using the Aeroballistic Research Facility Data Analysis System (ARFDAS),[8] whereas CADRA is also used in the trajectory matching process for the HFFAF. Both ARFDAS and CADRA use a nonlinear numerical integration technique[9] for the trajectory fitting process.

Models and Test Conditions

During the past few years, several different blunt-body atmospheric entry configurations have been tested. These were as follows:

1) The Huygens Probe, which is presently in route to Saturn as part of the Cassini mission, will enter the atmosphere of Titan (Saturn's largest moon) in late 2004 to accomplish measurements of the atmosphere. Two variations of this probe were tested, one having a base cavity.

2) An AFRL modification to the Huygens probe having a spherical base is also a configuration.

3) Another is the Mars Micro Probe, two of which were lost along with the main polar lander attempting to land on the surface of the planet in December 1999. If successful, these would have injected a probe into the subsurface to collect samples for on-site examination.

Table 1 Model physical properties

Model	Mass, g	Iy, g cm^2	Xcg/D
Huygens	a) 320	610	0.180
	b) 340	540	0.175
Huygens (hemispherical base)	374	1030	0.179
Mars Micro Probe	503	1410	0.267
Mars Probe (flat base)	450	1500	0.293
Stardust	a) 704	2320	0.350
	b) 730	2180	0.331
	c) 747	2350	0.364
(HFFAF)	d) 86	63	0.335
(HFFAF)	e) 11	11	0.335
Genesis	633	1990	0.343

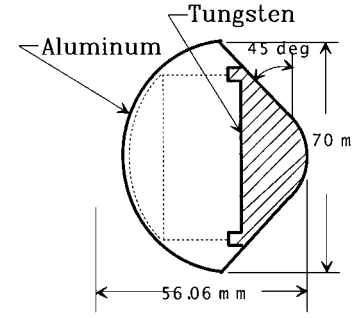

a) Mars Micro Probe

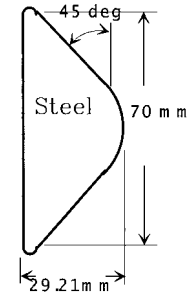

b) Mars Micro Probe with flat base

Fig. 3 Sketch of Mars Micro Probe and probe with flat base.

4) An AFRL modification to the Mars Micro Probe having a flat base is also included as a configuration.

5) Stardust Sample Return Capsule (SRC), launched in Feb. 1999, is presently on a 7-year mission to collect samples from the tail of a comet and return them to Earth. Five variations on this capsule configuration were tested. Three 70-mm-diam variations having different center of gravity locations were tested. Also, two NASA 35-mm-diam variations having different masses were tested at reduced atmospheric pressures in order to determine potential Reynolds-number effects.

6) Genesis Sample Return Capsule (SRC) was launched in Aug. 2001 on a 3-year mission to collect samples of the solar wind (atoms and ions emitted from the Sun) and return them to Earth.

Sketches of the various configurations are shown in Figs. 2–5 and a table summarizing the physical characteristics of the various subscale models are presented in Table 1. Because these blunt entry configurations have high drag characteristics, all of the models, except those launched at reduced atmospheric pressures (low Reynolds numbers), were purposely designed to be relatively massive in order to minimize the deceleration experienced during the flights in the facility.

The base of the Genesis SRC can be approximated by a hemisphere as indicated by the effective radius shown in the sketch of Fig. 5. Also, note that the center of this radius is located well ahead of the model's center of gravity. This will be discussed again later in the paper.

The models launched in the ARF had a design diameter of 70 mm. However, because of machining and construction tolerances the

Table 2 Overall test conditions

Model	Mach-number range	Angle-of-attack range, deg	Reynolds-number range, $\times 10^{-6}$
Huygens	1.0–2.8	0–30	1.99–5.57
Huygens (hemispherical base)	1.8	0–20	3.58
Mars Micro Probe	0.7–1.5	0–20	1.39–2.99
Mars Probe (flat base)	1.2–1.5	0–20	2.39–2.99
Stardust			
ARF	1.2–2.8	0–30	2.39–5.57
HFFAF	1.5–2.5	0–15	0.22–1.80
Genesis	1.4–3.5	0–40	2.79–6.97

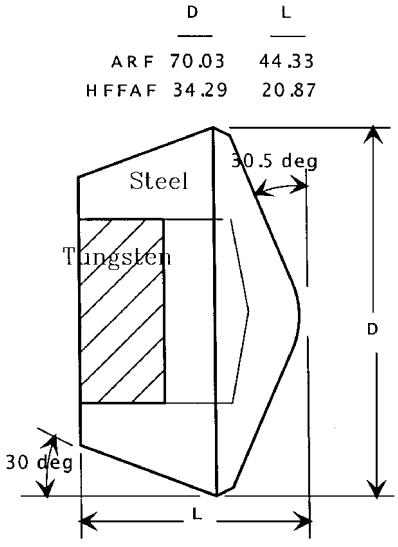

Fig. 4 Sketch of Stardust SRC. Note: The HFFAF models were homogeneous and were constructed from either steel or Lexan.

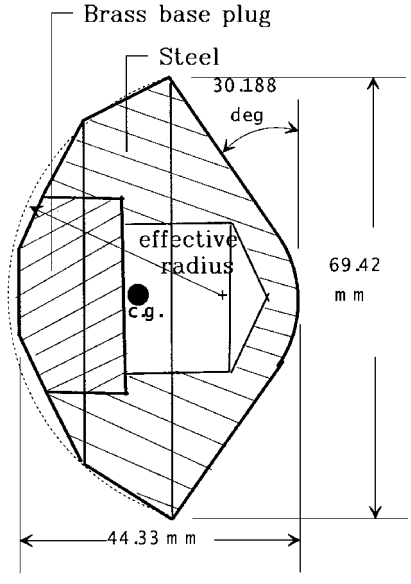

Fig. 5 Sketch of Genesis SRC.

diameters varied slightly with each configuration, about ± 0.03 mm. The models tested in the HFFAF were approximately half the size, $D = 34.3$ mm, of the ARF models. The models tested in the ARF were fired from a 76-mm smooth bore single stage powder gun. These tests were conducted at atmospheric conditions of about 21°C and 50% relative humidity. Barometric pressures were approximately 1020 mbar. Roll orientations and spin rates were measured on only a few of the models (ARF only) because it was shown that these blunt entry configurations tended to roll only slightly during flight and the analysis was insensitive to these low roll rates.

To achieve high initial angles of attack, some of the models in both facilities were purposely disturbed. This disturbance was accomplished by impacting the model into folded pieces of paper as they entered the instrumented portion of the facility. The 13 Stardust SRC models tested in the HFFAF were also launched using a single-stage powder gun, but with a bore diameter of 44 mm. The pressure in the HFFAF was varied to achieve the desired density. The reduced densities in conjunction with the smaller models resulted in the reduced Reynolds numbers. Table 2 summarizes the test conditions for each of the test programs.

Dynamic Stability Results

Huygens Probe and Modified Huygens Probe with Hemispherical Base

The typical motions obtained from testing the Huygens probe[10,11] are shown in Fig. 6. This figure illustrates that when the initial motion amplitude was high, the motion damped (Fig. 6a); when the initial amplitude was low, the motion grew (Fig. 6c); and when the initial amplitude was about 12 deg, the motion stayed constant (Fig. 6b). These motion characteristics were typical for both configurations of the Huygens probe (with and without the base cavity). This figure

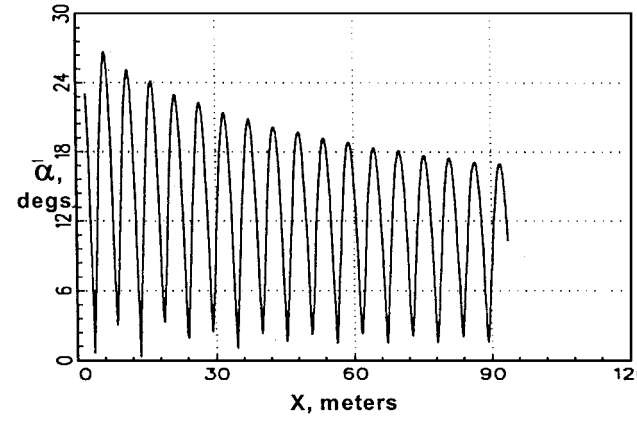

a) High angles

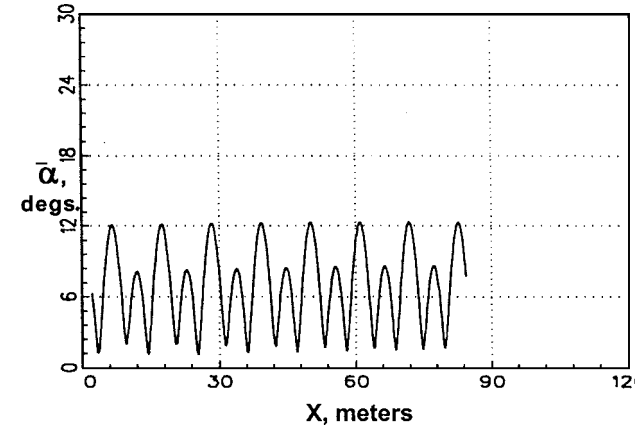

b) 12 deg

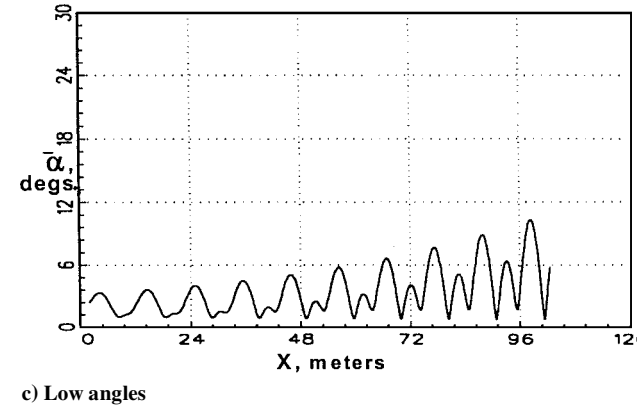

c) Low angles

Fig. 6 Typical Huygens Probe motion plots.

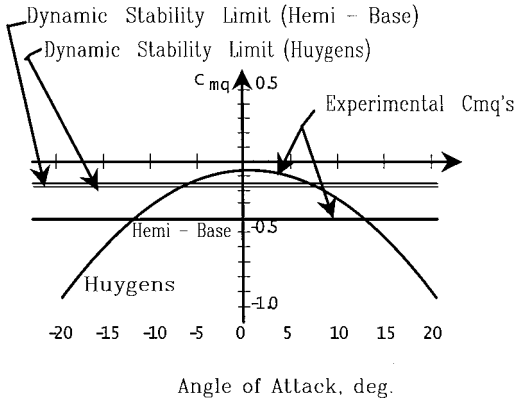

Fig. 7 Pitch-damping derivative vs angle of attack (Huygens Probe and probe with hemispherical base).

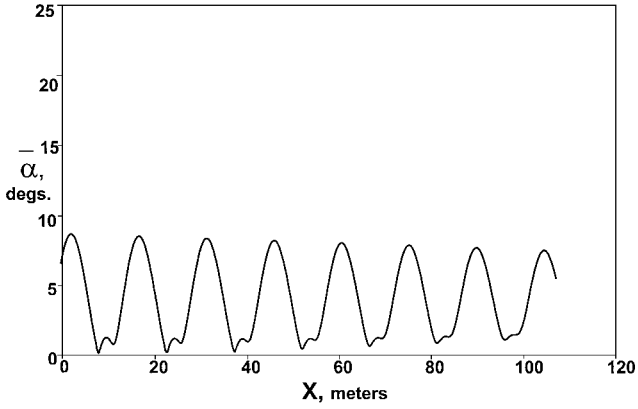

Fig. 8 Motion plot for modified Huygens Probe (hemispherical base).

describes a classic limit-cycle tendency and is caused by a nonlinear damping-in-pitch derivative *Cmq*. Figure 7 shows the nonlinearity in the measured *Cmq* and the Huygens stability limit computed using linear theory. This stability limit is calculated using the following relationship:

$$Cmq_l = \frac{C_{N\alpha} - 2C_D}{mD^2 / I_Y} \tag{1}$$

$C_{N\alpha}$ and C_D are obtained from the trajectory analysis. If *Cmq* is above the stability limit, the motion amplitude will increase. However because *Cmq* is decreasing with increasing angle-of-attack, the motion reaches a point where *Cmq* crosses the stability limit after which the model begins to become dynamically stable and the motion amplitude tends toward a limit cycle.

After testing the Mars Micro probe, discussed in the next section, it was suspected that the Huygens limit cycle of approximately 12 deg was related to the relative flat-base shape of this configuration. Therefore, additional models were constructed and tested with hemispherical bases.[12] The radius of the hemispherical base was defined as originating at the model's center of gravity. A typical motion from one of these flights is shown in Fig. 8, indicating that although the motion is damping slowly the amplitude is decreasing. This result indicates that *Cmq* is below the stability limit throughout the angle-of-attack range. Again the measured *Cmq* level for the hemispherical-based configuration, also shown in Fig. 7, confirms this result. In fact, no nonlinearity in the experimentally determined *Cmq* was detected for the hemispherical-based configuration.

Mars Micro Probe and Modified Micro Probe with Flat Base

The two primary purposes of testing the Mars Micro Probe were to determine the angle of attack and velocity as the probe impacted the surface of Mars. Achieving these purposes meant determining the magnitude of the limit cycle at impact. Although not shown here, the models were dynamically stable throughout the angle-of-attack and Mach-number range tested, and no limit cycles were found.

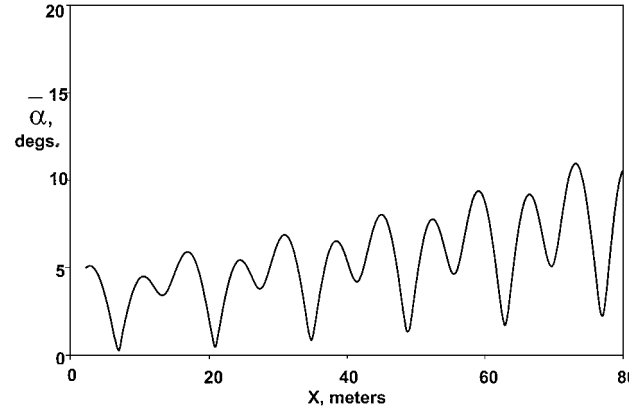

Fig. 9 Motion plot for modified Mars Micro Probe (flat base).

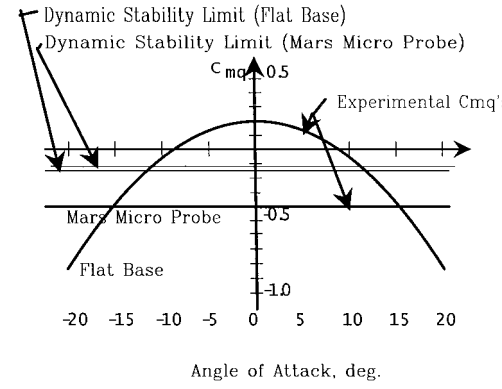

Fig. 10 Pitch-damping derivative vs angle of attack (Mars Micro Probe and probe with flat base).

Although these test flights were generally at lower Mach numbers than the other configurations because the impact velocity is subsonic, it was suspected that the hemispherical base on this configuration was the primary contributor to the model's dynamic stability. This suspicion was derived from Sammond's conclusions as reported in Ref. 1. Therefore additional models were constructed and tested with flat bases to investigate this suspicion. At that time it was also decided to construct and test the modified Huygens models with hemispherical bases, and those results were shown and discussed in the preceding section.

A typical motion plot for the flat-based Mars Micro Probe is shown in Fig. 9, and once again the model is dynamically unstable at the low angles of attack. These results and the results of the Huygens models with and without flat bases certainly indicate that the flat-base geometry is the primary cause of the low-angle-of-attack dynamic instability experienced by this class of configuration.

The experimentally determined *Cmq* values for the Mars Micro Probe and the flat-based modification are shown in Fig. 10. Again the *Cmq* limit values, calculated using Eq. (1), are shown in that figure confirming that the Mars Micro Probe is dynamically stable throughout the angle-of-attack range and that the flat-based configuration tends to a limit cycle of about 12 deg.

Stardust Sample Return Capsule

Typical motion patterns, as obtained in the ARF, for the Stardust SRC are shown in Fig. 11. These models had a limit cycle between 25 and 30 deg, and this did not appear to vary significantly with small changes in center-of-gravity positions, Xcg/D of 0.33 to 0.37, that were evaluated during this test program.[13]

The dynamic stability derivative data vs angle of attack for the Stardust configuration, as measured in the ARF, are shown in Fig. 12. Here we are only showing the positive side of the angle-of-attack curve, and a mirror image side exists for the negative angles of attack. Because the linear theory *Cmq* limit value is about −0.165

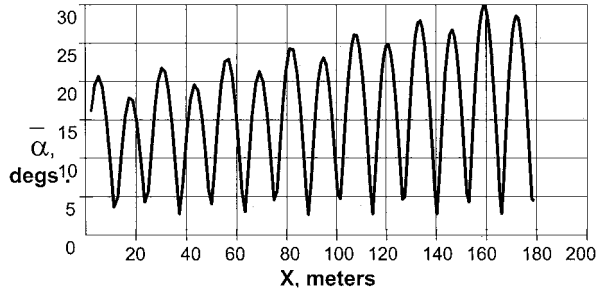

a) Average Mach number = 1.4

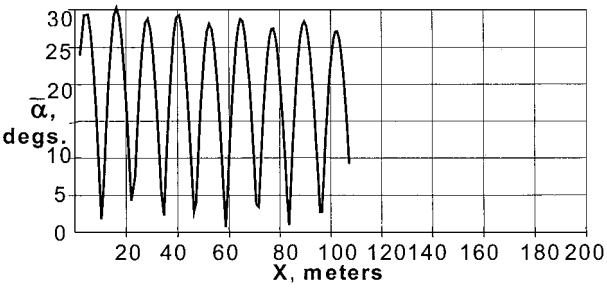

b) Average Mach number = 2.4

Fig. 11 Typical Stardust SRC motion plots.

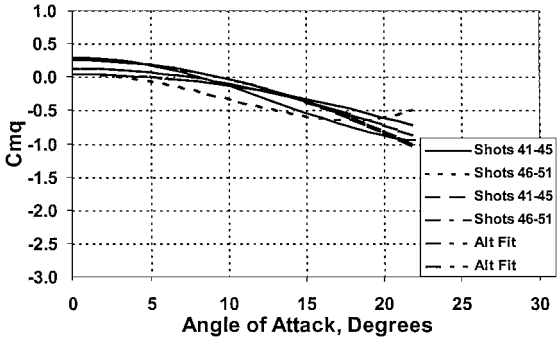

Fig. 12 Stardust SRC pitch-damping derivative vs angle of attack (as measured in the ARF).

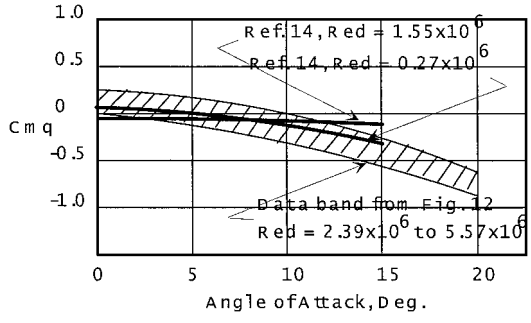

Fig. 13 Effect of Reynolds number on the Stardust SRC pitch-damping derivative.

and only varies slightly with Mach number and angle of attack, it would appear that this model should have become dynamically stable some where above 8–13 deg. However, as mentioned, the motion plots indicate a limit cycle between 25–30 deg.

Although the models used in the present tests were much smaller than their full-scale counterparts, the test Reynolds numbers were significantly higher than flight because of the flight altitudes and/or the various planetary atmospheres. Therefore, as already indicated, this configuration was chosen to investigate potential Reynolds-number effects in the Ames HFFAF.[14] The results of those tests are shown in Fig. 13 along with the comparisons of the ARF results, shown in Fig. 12, for the same configuration at significantly higher Reynolds numbers. These results illustrate two basic conclusions. First, the pitch damping as measured in both facilities is in good agreement. Second, there is a negligible Reynolds-number effect on the dynamic stability of these blunt bodies, at least for the range of Reynolds numbers tested.

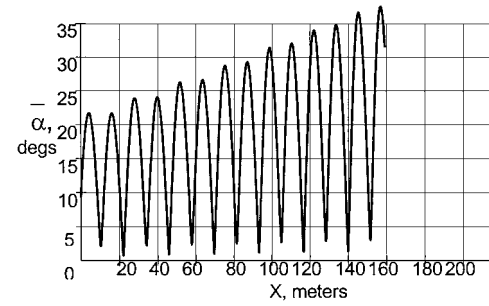

a) Average Mach number = 1.4

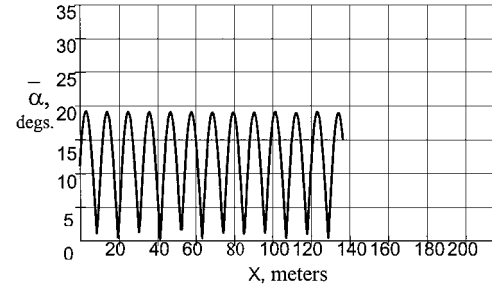

b) Average Mach number = 3.5

Fig. 14 Typical Genesis SRC motion plots.

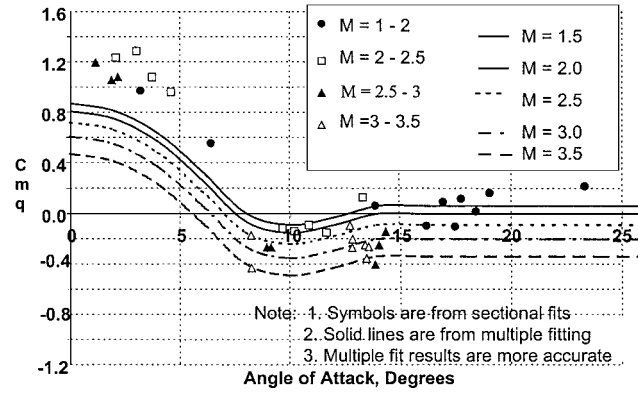

Fig. 15 Genesis SRC pitch-damping derivative vs angle of attack.

Genesis Sample Return Capsule

Typical angular motions resulting from the free-flight tests of the Genesis SRC[15] are illustrated in Fig. 14. Once again the total angle of attack is plotted vs distance flown. This figure shows that the subscale models of the Genesis SRC are also dynamically unstable at low yaw levels, especially at Mach numbers below 2.5 (Fig. 14a). However the rate at which the motion is undamped appears to be a function of Mach number. Note the difference in damping trends between the lower Mach number (Fig. 14a), which is at 35-deg angle of attack and still growing rapidly, whereas the model at the higher Mach number (Fig. 14b) might be approaching a limit cycle of approximately 20-deg angle of attack. It is possible that the model at the highest Mach number is not approaching a limit cycle in the classic sense; but that whatever the existing initial amplitude the motion would have continued at about that level. Nevertheless, the dynamic instability is obviously significantly greater at the lower Mach-number conditions, and for those conditions no limit cycle is apparent below 40 deg.

Figure 15 shows the experimentally measured pitch damping derivative data vs angle of attack. The mathematical aerodynamic model that originally existed within ARFDAS could not accurately model this nonlinearity. However, using the sliding sectional fit

option in ARFDAS, the general form of the pitch-damping derivative was input and form factored to best match the experimentally measured trajectories. Plotted in this figure are the relevant curves from this form-factored fit along with the sectional fitting results. The curves for the various Mach-number regimes represent the best estimates of the pitch-damping derivatives over the angle-of-attack range.

The linear theory dynamic stability limit for this model was computed and is about -0.175 and only varies slightly with Mach number and angle of attack. Therefore, if *Cmq* is less than -0.175, the model's angular motion should damp and greater than -0.175 the motion should grow. The data shown in this figure indicate that the models are highly dynamically unstable at the lower angles of attack possibly becoming stable between 8–15 deg and then becoming unstable again at the higher angles for the lower Mach numbers. However, the models remain stable at the higher Mach numbers. This observation is consistent with the motion plots shown in Fig. 14, and there seems to be considerable similarity with the Stardust configuration discussed in the preceding section. It is believed that the large dynamic instability associated with the Genesis configuration is at least partially caused by the forward location of the center of radius for the effective base radius (see Fig. 5). Therefore, it is suspected that if the distance between the model's c.g. and the location of the effective center of the base radius was decreased the dynamic instability would also decrease.

Although no limit cycles were found experimentally for the Genesis configuration, the aerodynamics for this configuration suggests that potential limit cycles exist. Because the pitch damping is a function of Mach number, there will be a different limit-cycle amplitude for each Mach number. The potential limit cycles were estimated using the approach given in Ref. 3. This approach assumes that the aerodynamics are not a function of Mach number. Hence when the approach of Ref. 3 is applied, the potential limit cycle that would occur at that Mach number is obtained. In the full dynamic case with aerodynamics that depends on Mach number, the amplitude will lag this limit-cycle amplitude. The limit-cycle amplitude can be estimated from the following equation:

$$\int_0^{\alpha_{\text{amp}}} \left[C_D - C_{L_\alpha} + \left(C_{m_q}\right)\left(\frac{mD^2}{I_y}\right)\right]\left(\frac{\mathrm{d}\alpha}{\mathrm{d}s}\right)\mathrm{d}s = 0 \qquad (2)$$

In general, the terms in the square brackets are a function of angle of attack. The slope of the lift coefficient curve is only weakly dependent on angle of attack and Mach number and hence is assumed to be constant. The pitch-damping term is a very strong function of angle of attack and must be considered. Therefore the experimental pitch-damping data presented in Fig. 15 were fitted with a polynomial from 0 to 14 deg angle of attack and splined to a constant value for angles of attack greater than 14 deg. Using this form, the preceding equation could be integrated in closed form. The integral is a higher-order polynomial that was solved numerically for the limit cycle amplitude α_{amp}.

The limit-cycle amplitudes resulting from this computation are plotted as a function of Mach number in Fig. 16. Here we see that the predicted limit-cycle amplitude at the higher Mach numbers $M \sim 5$ is small, i.e., below 5 deg. The predicted amplitude increases with decreasing Mach number, rising very rapidly below Mach number $\sim$3.5. This predicted behavior is consistent with the flight data as shown in Fig. 14a, where the average Mach number is 1.4 and also for the higher-Mach-number case, average $M = 3.5$, shown in Fig. 14b.

Precision of *Cmq* Measurements

The ability to determine *Cmq* from free-flight trajectory measurements depends on several factors. Some of these factors are 1) the precision to which the model's angular orientation measurements are obtained, 2) the magnitude of the angular motions, 3) the number of cycles obtained, 4) number of data points per cycle, 5) the applicability of the aerodynamic model assumed in the *Cmq* expansion vs angle of attack and Mach number, and 6) how much damping or undamping is actually present in the motions.

The ability to determine the angular orientations is a function of the configuration being tested. For most free-flight configurations with fineness ratio (L/D) of two or more, this measurement precision is about ± 0.1 deg. However, for the blunt configurations discussed in this paper where the fineness ratios are less than one the measurement precision is on the order of ± 0.5–0.7 deg. In fact, even to achieve this level of precision, considerable effort was expended to improve the existing angular orientation algorithms in CADRA.

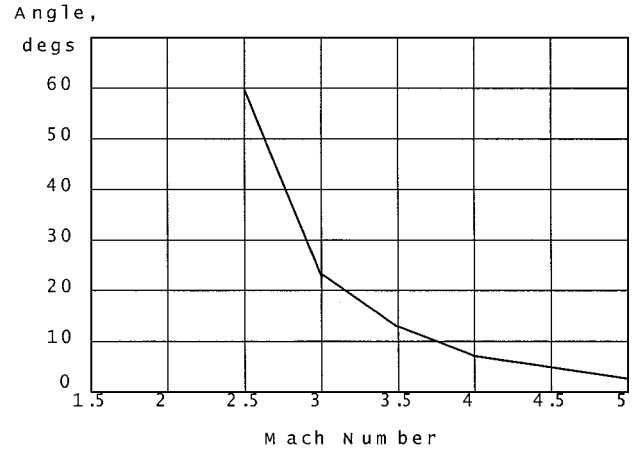

Fig. 16 Theoretical limit cycles.

For the present tests the motion amplitudes were significant. In general, the models launched at low angles of attack developed larger angles, and those launched at higher angles either continued to increase or approached a limit cycle. Therefore, the motion amplitudes were large enough and changing significantly such that *Cmq* could be reasonably determined. This result was true even though the measurement precision of the angles were degraded as a result of the blunt low fineness ratio configurations.

Also, although the two facilities used for these tests were of differing lengths and number of measurement locations, it is believed that adequate amounts of data were obtained in both, especially because multiple flights were analyzed simultaneously. Considering all of the preceding information it is estimated that the *Cmq* levels are accurate to ± 0.25. This value is derived from probable errors associated with the individual fits to the experimentally measured trajectories and is consistent with the levels presented for all of the configurations. Finally, it is certain that the angle-of-attack and Mach-number trends shown for the various configurations are good representations of their damping characteristics at least for atmospheric chemistries that are consistent with air.

Conclusions

A series of blunt-body atmospheric entry shapes have been tested. These tests covered a Mach-number range of subsonic to high supersonic 0.7–3.5, Reynolds numbers from 0.27×10^6 to 6.97×10^6, and angles of attack up to 40 deg. All of the configurations with "flat" bases demonstrated low-angle-of-attack dynamic instabilities, and most of these culminated in limit-cycle motions. The two configurations with hemispherical bases did not exhibit these low-angle-of-attack dynamic instabilities but were dynamically stable throughout the angle-of-attack range. The tests for the effects of Reynolds number on the Stardust configuration indicate that these effects are minimal, at least for the Reynolds numbers tested. The Genesis results, which covered a broader range of Mach numbers and angles of attack than the other configurations, demonstrated that the dynamic instability is highly dependent on Mach number.

The general conclusions can be summarized in the following statements. First, these blunt atmospheric entry configurations tend to have low angle-of-attack dynamic instabilities culminating in limit cycles. Second, the afterbody shape causes the dynamic instabilities. Hemispherical afterbodies with the radius located at the model's center of gravity eliminate the dynamic instability. This conclusion is identical to Sammond's conclusion in 1970 (Ref. 1). Third, the dynamic stability derivatives are a complex function of angle of attack and Mach number. At low Mach numbers $M < 2.5$, some configurations, i.e., Genesis, might also be unstable

at high angles of attack. Fourth, the theoretical limit cycles for the Genesis SRC were computed across the Mach-number range and are consistent with the experimentally measured motions. Fifth, the effect of Reynolds number appears to be minimal for these blunt bodies. Last, good agreement exists between the data obtained in the U.S. Air Force Aeroballistic Research Facility and the NASA Hypervelocity Free-Flight Aerodynamic Facility.

Acknowledgments

Many individuals were involved in these test programs, and the authors wish to especially acknowledge five persons for their efforts: first, John Krieger, Chief Technician in the Aeroballistic Research Facility (ARF), for accomplishing most of the tests reported on herein and for scanning and reading the film for the ARF tests; second, Leslie Yates for her support in incorporating updates to the Comprehensive Automated Data Reduction and Analysis System for these blunt configurations; and last, the sponsorship and guidance of Robert Mitcheltree and Neil Cheatwood, scientists at the NASA Langley Research Center, Hampton, Virginia, along with Eric Slimko, formerly at the Jet Propulsion Laboratory, Pasadena, California.

References

[1]Sammonds, R. I., "Transonic Static—and Dynamic Stability Characteristics of Two Large-Angle Spherically-Blunted High Drag Cones," AIAA Paper 70-564, May 1970.

[2]Chapman, G. T., and Yates, L., "Dynamics of Planetary Probes—Design and Testing Issues," AIAA Paper 98-0797, Jan. 1999.

[3]Chapman, G. T., and Yates, L., "Limit Cycle Analysis of Blunt Entry Configurations," AIAA Paper 99-1022, Jan. 1999.

[4]Kittyle, R. L., Packard, J. D., and Winchenbach, G. L., "Description and Capabilities of the Aeroballistic Research Facility," U.S. Air Force Armament Lab., AFATL-TR-87-08, Eglin AFB, FL, May 1987.

[5]Canning, T. N., Seiff, A., and James, C. S., "Ballistic Range Technology," Rept. 138-70, AGARD, Aug. 1970.

[6]Winchenbach, G. L., "Aerodynamic Testing in a Free-Flight Spark Range," Wright Lab., WL-TR-1997-7006, Eglin AFB, FL, April 1997.

[7]Yates, L. A., "A Comprehensive Aerodynamic Data Reduction System for Aeroballistic Ranges," Wright Lab., WL-TR-96-7059, Eglin AFB, FL, Oct. 1996.

[8]Fischer, M. A., and Hathaway, W. H., "ARFDAS Users Manual," U.S. Air Force Armament Lab., AFATL-TR-88-48, Eglin AFB, FL, Nov. 1988.

[9]Chapman, G. T., and Kirk, D. B., "A Method for Extracting Aerodynamic Coefficients from Free-Flight Data," *AIAA Journal*, Vol. 8, No. 4, 1970, pp. 753–757.

[10]Giraud, M., Berner, C., and Winchenbach, G. L., "Aeroballistic Investigation of Supersonic Hemispheric Shapes, Computation and Experiment," 16th International Symposium on Ballistics, Paper EB13, American Defense Preparedness Association, Sept. 1996.

[11]Berner, C., and Winchenbach, G. L., "A Numerical and Experimental Investigation of Generic Space Probes," AIAA Paper 98-0798, Jan. 1998.

[12]Chapman, G. T., Berner, C., Hathaway, W. H., Winchenbach, G. L., and Mitcheltree, R., "The Use of Spherical Bases to Eliminate Limit Cycles of Blunt Entry Vehicles," AIAA Paper 99-1023, Jan. 1999.

[13]Chapman, G. T., Mitcheltree, R., and Hathaway, W. H., "Transonic and Low Supersonic Static and Dynamic Aerodynamic Characteristics of the Stardust Sample Return Capsule," AIAA Paper 99-1021, Jan. 1999.

[14]Ramsey, A. L., and Chapman, G. T., "A Study of Reynolds Number Effects on Supersonic Flow over Blunt Bodies," AIAA Paper 2000-1010, Jan. 2000.

[15]Cheatwood, N., Winchenbach, G. L., Hathaway, W. H., and Chapman, G. T., "Dynamic Stability Testing of the Genesis Sample Return Capsule," AIAA Paper 2000-1009, Jan. 2000.

P. Weinacht
Associate Editor